ELECTRO-OPTICAL SWITCHES

Recently, there has been an increasing interest in the development of high-bit-rate systems for transmission of information, mostly data and video. These systems are becoming part of the information superhighway. The cornerstone of this revolution is the long-distance fiber optic links involving the gamut of interactive cable television, wireless communication, and the like, all of which require ultra-high-speed data transmission. Evidently, it is quintessential to increase the speed at which information can be processed and transmitted so as to use effectively the large bandwidth of the optical fiber gracefully provides.

Currently, both direct modulation of the laser diode and external modulation are being implemented towards wide-scale deployment in optical systems of signal transmission and processing (1). In a favorable comparison with directly modulated laser diodes, external modulators can have extremely low chirp, i.e., intensity modulation without frequency (wavelength) modulation. Electro-optic modulation has distinct advantages over the other mechanisms that can be used for external modulators. Furthermore, guided-wave electro-optic modulators, in which light is confined within a wave-guiding area of small dimensions, exhibit several advantages over their conventional bulk counterparts. The devices in the integrated-optic embodiment exhibit orders-of-magnitude wider bandwidth (faster switching times) and lower drive power. In addition, they are lightweight, miniature, immune to electromagnetic interference, and inherently compatible with optical fiber (2).

Efficient external guided-wave modulators have already been demonstrated with bandwidths up to 100 GHz and transistor–transistor logic (TTL) compatible drive voltages. Subsequent wavelength-division multiplexing of independent channels, each modulated at gigabit rates, can enable aggregate transmission rates in the terabit range. Therefore, optical systems based on efficient electro-optic modulators are highly desirable for many commercial and military applications including sensor systems (3), fiber optic telecommunication links (2,4), and microwave antenna remote detection systems (5).

A number of substrate materials have been studied in the past with a view toward their use in the mass production of integrated-optic components. As for electrooptic modulators, ferroelectrics (lithium niobate, lithium tantalate, etc.) and semiconductor alloys (InGaAs, InGaAsP, InGaAlAs, etc.) have been found to be the most suitable materials. Recently, there has been a significant effort in developing modulators in polymer materials which exhibit temporally stable electrooptic effects after poling in an external electric field. Currently, modulators in ferroelectrics take a substantial lead in practical use because of a favorable combination of the electro-optic properties, quality, and material cost, as well as a relatively simple fabrication process. Monolithic integration of modulators with optical sources appears to be very promising in light of the latest impressive results obtained with rare-earth-doped waveguide lasers in ferroelectrics.

When designing an electro-optic modulator (EOM), several characteristics are of special concern, including the drive voltage and power, bandwidth, insertion loss, and crosstalk (extinction ratio). Recently, in light of the rapid advancement of cable TV links, the linearity of the device transfer curve has also become an issue of utmost importance. The design of an EOM represents a rather complicated task because there exist a number of trade-offs relating two or more of the device characteristics. Hence, the requirements of a specific practical application where the modulator is to be employed should be considered in order to determine which parameters may limit the overall performance.

In this aticle, we present a review of the existing EOMs in terms of the operation principles and performance achieved to date rather than give a historical overview. We emphasize the schemes that show the strongest practical potential with some of them already advanced to the commercial stage.

MAIN CHARACTERISTICS OF ELECTRO-OPTIC MODULATORS

The electro-optic modulator is a device that impresses the information contained in the modulating electric signal onto an optical carrier. Any parameter of the optical wave—amplitude, phase, polarization or frequency—can be modulated. This article emphasizes guided-wave electro-optic *amplitude* (intensity) modulators, which are the largest and most developed class of integrated-optic EOMs. As follows from its name, an amplitude modulator varies the amplitude of the optical wave in the output channels via the application of an electric signal. The electro-optic switch is a specific case of the EOM that switches the optical power in a specific output channel between two discrete positions—on and off states—with the maximum and minimum transmission. Throughout this article, we use the term *electro-optic modulator* to include the electro-optic switches unless stated otherwise.

The waveguide structure of the EOM is composed of channel (two-dimensional mode confinement) and/or planar (one-dimensional mode confinement) integrated-optic waveguides formed in an electrooptic material. In its simplest form, the electrode structure of the EOM is a pair of coplanar electrodes, separated by a several-micron-wide gap and delineated on the same surface of the sample, in close proximity to the waveguides. Due to the small lateral dimensions of integrated-optic waveguides and the matching interelectrode gap, voltages as low as several volts can create electric fields sufficient for deep optical modulation.

Typically, two mechanisms of modulation are used in EOMs. The first modulation mechanism commonly used is based on the linear electro-optic (Pockels) effect. In this case, the applied voltage produces a change in the real part of the refractive index that is proportional to the applied voltage. The electro-optically induced index change translates into an electro-optical phase shift for the guided mode. The phase shift is subsequently converted, by some means, into intensity modulation. Alternately, modulation of the real part of optical index can be directly converted into intensity modulation by changing the cut-off conditions for the guided mode. The second modulation mechanism is the direct modulation of the attenuation coefficient for the optical wave via modulation of the imaginary part of the refractive index as implemented in electroabsorption modulators (see Chap. 16 in Ref. 2).

The modulation characteristic (i.e., optical output versus electric input) is the transfer function (curve) of the EOM. Main performance characteristics of the device can be determined from its transfer curve. The slope of the transfer curve determines the modulation efficiency. The ratio of the maximum to the minimum of the curve determines crosstalk (extinction ratio). In other words, crosstalk is defined as the ratio of the power remaining in the output channel from which the light is switched to that in the channel to which the light is switched. The difference between the voltages corresponding to adjacent extrema (minimum and maximum) of the transfer curve is the switching voltage (i.e., the voltage required to switch light from one channel to another). The dependence of the switching voltage on the frequency of the modulating electric signal is the frequency response of the device.

Clearly, the device design should be aimed at achieving a high-speed switch with low drive power and crosstalk. This task is, in many instances, rather complicated in view of the multiple structural parameters to be optimized (parameters of waveguide and electrode, material composition, etc.) and the numerous trade-offs that exist among different performance characteristics. For instance, a trade-off is known to exist between the maximum speed and the drive power. High-speed operation typically requires short interaction lengths that result in increased voltages. We have included a section in this article that describes the major trends in the development of EOMs and pinpoints the aforementioned trade-offs.

MODULATORS INCORPORATING COUPLED WAVEGUIDES

There are a variety of EOMs comprising coupled-waveguide structures. In this section, the most typical schemes such as the 2×2 directional coupler, 1×2 (Y-fed) directional coupler, and BOA (zero-gap) switch are described. These devices have been used both individually and as the building blocks of multichannel switching matrices (6).

2×2 Directional Coupler

The waveguide structure of the conventional 2×2 directional coupler/switch (7) is composed of two single-mode channel waveguides placed in close proximity to each other (Fig. 1) so that the evanescent tails of the modes overlap. The waveguides comprising the switch are electromagnetically coupled in the sense that they can exchange optical power between each other. For the most efficient power transfer, the waveguides must be phase matched (i.e., their propagation must be identical for at least one wavelength). In this case, light launched into one of the channels couples over to the other,

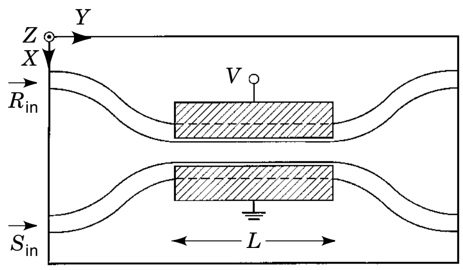

Figure 1. Schematic of directional coupler. Lateral dimensions are shown to an enlarged scale. Exchange of optical power between the coupled waveguides is controlled by the external voltage V applied to the electrodes.

as the modes propagate along the interaction length. After some distance ℓ, called the coupling length, all the light from the first channel is transferred to the other. For typical single-mode waveguides in the near infrared (IR) region, a coupling length of a few millimeters requires an inter-waveguide gap of several microns. Therefore, input/output waveguide bends should be used in a practical device with the maximum output channel separation of about 125 μm to 150 μm to allow for device pigtailing to single-mode fibers.

The power exchange between the coupled waveguides is sensitive to the phase mismatch between them and, hence, can be controlled by applying an external voltage so as to change the propagation constants of the waveguides. Upon increasing the voltage, the originally phase-matched waveguides become more and more dephased. This leads to an increasingy suppressed power transfer between them until all the light remains in the input channel it was launched into. Thus, the device can function as an electrooptical modulator/switch.

The electrode stucture of the device should be chosen in such a way that the maximum electrooptic coefficient of the material is exploited. For example, a two-electrode structure with electrodes over the coupled waveguides provides the most efficient, push–pull configuration (also known as the COBRA configuration) for a switch in Z-cut $LiNbO_3$. For this crystal orientation, light of TM-polarization and the vertical component of the applied electric field are used in order to benefit from the largest electrooptic coefficient, r_{33}, yielding the lowest switching voltage. The latter is also dependent on the overlap between the mode intensity profile and the electric field distribution. The electrooptical integral should, therefore, be maximized by properly adjusting the waveguide and electrode dimensions as well as positioning the electrode structure with respect to the waveguide. These requirements deem, in particular, a 2×2 switch in X-cut $LiNbO_3$ to be an inferior alternative to its Z-cut counterpart, especially for high-speed applications. Indeed, a three-electrode structure would be required to implement push–pull operation in X-cut with a fairly narrow center electrode which is lossy at high frequencies.

The transfer curve of the directional coupler (DC) is governed by a matrix expression that relates the input and output optical fields. The matrix equation can be derived by solving the coupled-mode equations; for the case of weak coupling between nearly identical waveguides it is given by (7,8):

$$\begin{bmatrix} R_{out} \\ S_{out} \end{bmatrix} = A \begin{bmatrix} R_{in} \\ S_{in} \end{bmatrix} = \begin{bmatrix} a_{11} & a_{12} \\ a_{21} & a_{22} \end{bmatrix} \begin{bmatrix} R_{in} \\ S_{in} \end{bmatrix} \tag{1}$$

where $R_{in}(S_{in})$ and $R_{out}(S_{out})$ are the optical fields in the input (and output) channels (Fig. 1). The coefficients of matrix A are given by the following expressions:

$$\begin{aligned} a_{11} &= \cos\left(L\sqrt{\kappa^2+\delta^2}\right) + j\frac{\delta}{\sqrt{\kappa^2+\delta^2}}\sin\left(L\sqrt{\kappa^2+\delta^2}\right) \\ a_{12} &= -j\frac{\kappa}{\sqrt{\kappa^2+\delta^2}}\sin\left(L\sqrt{\kappa^2+\delta^2}\right) \\ a_{21} &= a_{12} \\ a_{22} &= a_{11}^* \end{aligned} \tag{2}$$

where L is the interaction length, $\kappa = \pi/2\ell$ is the coupling coefficient; and $\delta = (\beta_1 - \beta_2)/2 = \Delta\beta/2$ represents the mismatch between the propagation constants (β_1 and β_2) of the waveguides. For the linear electro-optic effect, δ and $\Delta\beta$ are proportional to the voltage applied to the electrodes. In Eqs. (1) and (2), residual coupling in the input/output bends is neglected.

The performance of the switch is best illustrated by its switching diagram (Fig. 2) in terms of the normalized parameters L/ℓ and $\Delta\beta L/\pi$. The diagram is obtained by using Eq. (2) and requiring the power in the cross output channel to be zero for the bar state. Likewise, zero power in the bar output channel corresponds to the cross state. In the diagram, the cross and bar state are denoted by the symbols ⊗ and ⊜, respectively. If the interaction length of the coupler is equal to exactly one coupling length ($L = \ell$), the cross state is achieved. When the applied voltage increases, the operating point of the device moves along the horizontal direction in

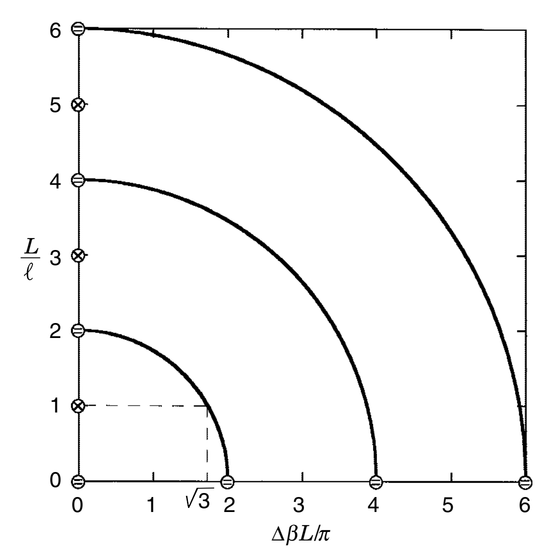

Figure 2. Switching diagram of directional coupler. Cross and bar states are shown by symbols ⊗ and ⊜, respectively. The coupler is chosen to be exactly one coupling length long. For no applied voltage, the cross state at $L/\ell = 1$ on the vertical scale is achieved. With increasing applied voltage, the operating point of the device moves horizontally (dashed straight-line segment) and intersects the circle corresponding to the next bar state.

Fig. 2 and intersects the circle corresponding to the next bar state. From the diagram, the switching condition can be determined to be $\Delta\beta L = \sqrt{3}\pi$. As seen from the diagram, even though the bar state is electro-optically tunable, the cross state is not. As a result, if the coupling length of the fabricated device deviates from the designed value, the crosstalk deteriorates and cannot be remedied by applying a dc bias. As a result, typical experimental values of crosstalk are in the range from -20 dB to -25 dB.

The impact of fabrication imperfections on crosstalk can be substantially reduced, if not eliminated completely, by invoking the principle of phase reversals as illustrated in Fig. 3(a) for the case of the $\Delta\beta$-switch with electrode reversals (8). As seen, the waveguide structure of this switch is the same as that of the conventional directional coupler with uniform electrodes. However, the electrode structure of the $\Delta\beta$-reversal DC incorporates two (or more) sections of alternating polarity. The corresponding switching diagram (shown in Fig. 4 for a two-section $\Delta\beta$-switch) indicates that both the bar and cross state are now electro-optically tunable. In this case, even if the actual value of L/ℓ deviates from the optimum value of 2 required for the bar state, one can first achieve the cross state by applying a dc bias and moving along the horizontal dashed line in Fig. 4. Switching between the cross and the next bar state can then be accomplished by applying a modulating ac signal.

In practice, the crosstalk of a practical $\Delta\beta$-reversal DC is still limited, typically between -30 dB and -40 dB, because of device asymmetry, residual coupling in the input/output bends, fluctuations of waveguide index profile along the propagation direction, scattering and recoupling of light (coherent coupling effects and the like), and possible misalignment between the electrode structure and the waveguide. Application of alternating voltages of unequal magnitudes may partially compensate for the impact of these factors. Adding more sections provides more flexibility and is also known to lower crosstalk at the expense of having to use more independent voltages.

The high-speed operation of $\Delta\beta$-switches can be established by carefully designing the electrode structure, by capacitively loading the separate electrode sections to a single transmission coplanar microstrip line, or by replacing electrode reversals with domain reversals (9). In the latter case, only a uniform traveling-wave electrode structure (see section entitled "Optimization of High-Speed Operation") is needed as illustrated in Fig. 3(b), which is fully compatible with a single microwave source.

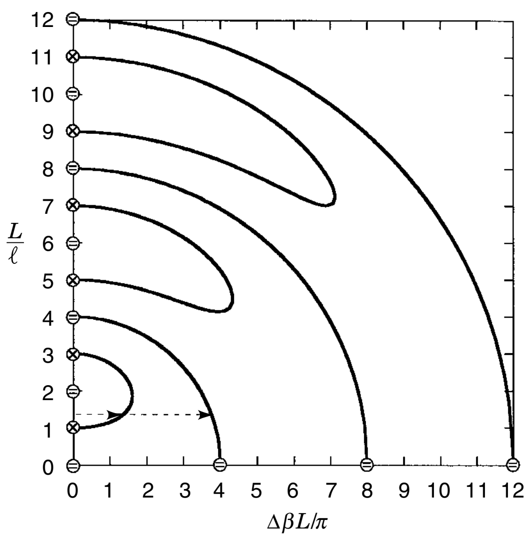

Figure 4. Switching diagram of two-section $\Delta\beta$-reversal directional coupler (8). Even when the actual value of L/ℓ deviates from the optimum value of 2 corresponding to the bar state, both the cross and bar states can be achieved by properly adjusting the applied voltage. An example when L/ℓ is between 1 and 2 is illustrated with the dashed line segments.

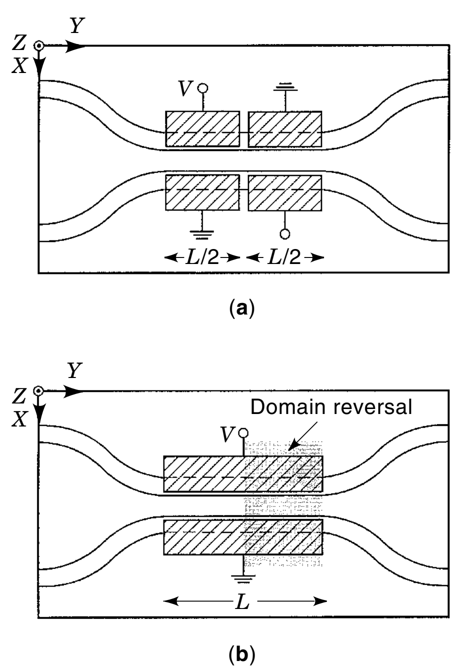

Figure 3. Directional coupler in $\Delta\beta$-reversal configuration: segmented electrodes (a) and the domain-reversed version (b) (8). The latter achieves the $\Delta\beta$-reversed operation with a uniform electrode structure.

1 × 2 (Y-fed) DIRECTIONAL COUPLER

The waveguide structure of the 1 × 2 DC (10) consists of a single-mode input waveguide joining a symmetric Y-junction with two output transitions (Fig. 5). The branches of the Y-

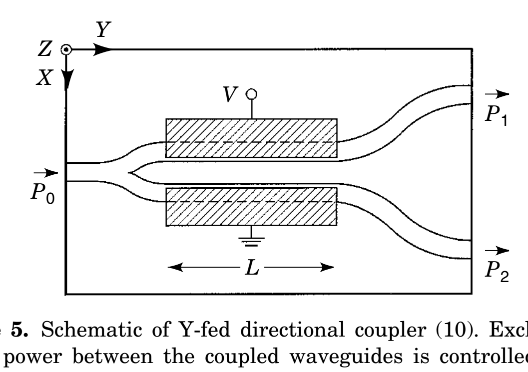

Figure 5. Schematic of Y-fed directional coupler (10). Exchange of optical power between the coupled waveguides is controlled by the external voltage V applied to the electrodes.

junction represent two identical, parallel, single-mode, coupled waveguides. The configuration of the electrode structure is, as always, dictated by the requirement that the largest electrooptic coefficient available in the material be used. For example, the uniform electrode structure shown in Fig. 5 corresponds to a device fabricated in Z-cut $LiNbO_3$. In this case, TM (transverse magnetic) polarized light will be modulated by the vertical component of the electric field via the largest electro-optic coefficient r_{33}.

In the absence of the modulating voltage, light coupled into the input waveguide splits evenly between the coupled waveguides. Due to the symmetry of the device, light at the output is equally split between the two output arms regardless of the length of the coupled-waveguide section. No electric bias is needed to set the operating point of the modulator to the middle of the transfer curve (i.e., the quadrature point). The Y-fed coupler represents, therefore, a structure that allows "built-in" linear operation in the absence of fabrication deviations. Another attractive feature of the 1×2 directional coupler is that it operates under nearly equal average powers in its arms, thus offering improved resistance to optical damage.

When an external voltage is applied, a phase mismatch between the coupled waveguides is introduced, eliminating the device symmetry and producing uneven splitting of the output light. An expression for the modulation characteristic can be obtained by using the coupled-mode theory. Under the assumption of abrupt output transitions (negligible coupling in the section following the coupled waveguides) and a lossless, weakly coupled waveguide structure, the transfer curve is governed by (10)

$$\frac{P_1}{P_0} = \frac{1}{2} - \frac{\kappa\delta}{\kappa^2+\delta^2}\sin^2\left(L\sqrt{\kappa^2+\delta^2}\right) \qquad (3)$$

where P_0 is the optical power in the input waveguide; P_1 is the power in one of the output waveguides (from the law of energy conservation, the power in the other channel is $P_2 = P_0 - P_1$).

Figure 6 shows the transfer curve of the 1×2 DC with L/ℓ being a parameter. As seen, 100% modulation depth (i.e., $P_1/P_0 = 1$ for some value of the applied voltage) can only be achieved if $L/\ell = 1/\sqrt{2}$ (10) resulting in the switching condition $\Delta\beta L = \sqrt{2}\pi$. As seen, the 1×2 coupler has a lower switching voltage than a 2×2 directional coupler of the same interaction length L. This fact is the result of the equal splitting of power at the input of the coupled-waveguide section in the 1×2 DC. Deviations from the optimum value $L/\ell = 1/\sqrt{2}$ result in a reduced modulation depth and, hence, deterioration of crosstalk. A crosstalk of ~ -20 dB was demonstrated in a 1 cm long device operating at $\lambda = 1.3\ \mu$m with a switching voltage of $\sim$7 V (10). As with the case of the 2×2 DC, $\Delta\beta$ electrode reversals have been proposed to reduce the sensitivity of crosstalk to fabrication imperfections that affect the value of ℓ in actual Y-fed couplers (11).

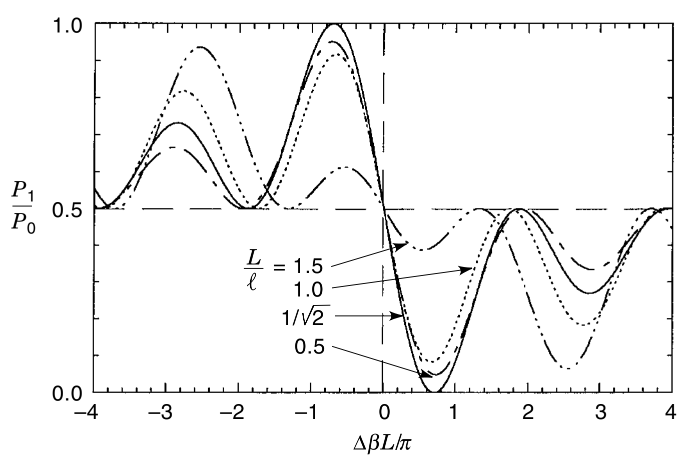

Figure 6. Modulation curves of Y-fed directional coupler with L/ℓ being a parameter (10). Full modulation (100% modulation depth) is achieved when $L/\ell = 1/\sqrt{2}$ (solid curve). Deviation of L/ℓ from $1/\sqrt{2}$ results in a reduced modulation depth.

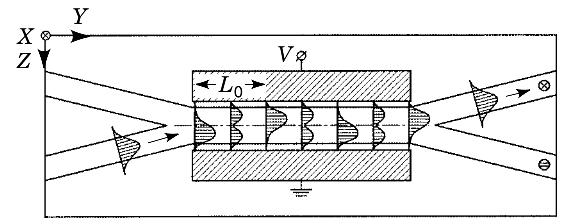

Figure 7. Schematic of BOA modulator (12). The phase between the two modes of the wide section changes as they propagate due to different propagation constants. The modes interfere with each other to produce a field distribution with its shape changing along the propagation direction. The relative phase and the field profile are controlled by applied voltage V to enable tunable splitting of optical power between the output channels.

BOA Switch

The waveguide structure of the BOA (bifurcation optique active) switch (12) is composed of intersecting single-mode input/output channels and a wider, two-mode channel connecting them (Fig. 7). In fact, the structure can be regarded as a directional coupler with a zero interwaveguide gap. The principle of device operation is the electro-optically controllable interference between the modes of the wide waveguide. Figure 7 corresponds to a switch in X-cut $LiNbO_3$. The necessary modulating electric field is created by a pair of uniform electrodes alongside the two-moded waveguide section. The horizontal component of the electric field and TE (transverse electric) polarized light should be used for the maximum efficiency. Note that the electro-optic change in refractive index is symmetric with respect to the Z axis, as opposed to the case of the 2×2 coupler where an antisymmetric electrooptic perturbation is used (electric field is directed downward in one of the coupled waveguides and upward in the other). In a sense, the BOA switch may be considered as a zero-gap coupler that uses $\Delta\kappa$-modulation instead of $\Delta\beta$-modulation.

If light is launched, for example, into the lower input waveguide in Fig. 7, then the field distribution at the beginning of the two-moded section is localized mostly in its lower half. The field is a combination of the fields of the fundamental (symmetric) and first-order (antisymmetric) mode excited with different amplitudes and phases. As these modes propagate along the structure, the phase shift between them increases because of the difference between their propagation constants. After some distance, called the beat length L_0, the phase shift increases by π with respect to its initial value. As a result, the field distribution produced by the interfering waves flips with respect to the horizontal axis of symmetry with the maximum being now in the upper half of the waveguide. If the two-moded section ends at this position and is followed by an output Y junction, light will go mostly to the upper channel. Similarly, if the length of the two-moded section is twice the beat length, light will be switched to the lower channel. By applying a voltage to the electrodes, we can change the propagation constants of the symmetric and antisymmetric modes at different rates and, therefore, modulate the phase shift between the modes. By tuning the phase shift to an odd and even multiple of π, switching of light between the channels can be achieved for an arbitrary interaction length.

The transfer curve of the device is a sine-squared function of the total phase shift $\Delta\Phi$ (13):

$$P_{\ominus} = \cos^2(\Delta\Phi/2)$$
$$P_{\otimes} = \sin^2(\Delta\Phi/2) \tag{4}$$

$\Delta\Phi$ is accumulated over both the two-moded section (of length L) and input/output Y junctions:

$$\Delta\Phi = (\beta_1 - \beta_2)L + \int_{\text{in}} [\beta_1(z) - \beta_2(z)]\,dz + \int_{\text{out}} [\beta_1(z) - \beta_2(z)]\,dz \tag{5}$$

The first term on the right side of Eq. (5) is the phase shift that accumulates over the two-moded section (of length L) with a constant difference between the propagation constants β_1 and β_2 of the fundamental and antisymmetric modes, respectively. The second and third terms correspond to the phase shifts between the local normal modes accumulated over the input and output Y junctions, respectively, on account of the residual coupling in the branching sections.

As can be seen from Eq. (4), the switching voltage V_s is determined by the condition $\delta[\Delta\Phi(V_s)] = \pi$, which can be rewritten with the use of Eq. (5) as

$$\delta(\beta_1 - \beta_2)L = \pi \approx -\frac{\pi}{\lambda} n^3 r \frac{V_s}{G}(\Gamma_1 - \Gamma_2)L \tag{6}$$

where λ and n are the wavelength and bulk refractive index of the optical wave, r denotes the effective electro-optical coefficient, G is the interelectrode gap, and Γ_1 and Γ_2 represent the overlap integrals between the electric field created by the electrode and the intensity profile of the symmetric and antisymmetric modes in the two-moded section, respectively.

First experimental devices in Y-cut $LiNbO_3$ with 5 mm long electrodes required a ~26 V voltage to switch light at $\lambda = 0.5145$ μm between the output channels with a crosstalk of ~−18 dB (12). Afterwards, the modulation efficiency was increased in a Z-cut $LiNbO_3$ switch with a symmetric three-electrode structure that maximized the difference between the electrooptical integrals Γ_1 and Γ_2 for the two interfering modes (13). Crosstalk lower than −28 dB was measured.

INTERFEROMETRIC MODULATOR

The interferometric modulator, known as the Mach–Zehnder interferometer (MZI), is the most widely used type of EOM (14). Due to its simple design and a favorable combination of performance characteristics, MZI has received much attention. Currently, MZI is one of the most advanced types of guided-wave devices, available commercially from several manufacturers (15).

In its simplest embodiment, MZI features a 1 × 1, on–off amplitude modulator/switch (Fig. 8). Light launched into a single-mode input waveguide splits equally between the arms of a symmetric input Y junction. The waves propagating along the interferometer arms converge and interfere in the second Y-junction. If the relative phase shift between the waves is an odd multiple of π, the optical field in the converging arms represents the antisymmetic (first-order) mode of the output Y junction. This mode is not supported by the following single-mode section and radiates into the substrate. On the other hand, when the phase shift between the waves equals an even multiple of π, only the even mode of the output Y junction is excited which converts, with little loss, into the fundamental mode of the output single-mode section. The phase between the interfering waves is controlled by the applied voltage. If the electrode configuration is designed in such a way that the phase shift induced in one arm is equal in magnitude and opposite in sign to that in the other arm, the relative phase shift between the arms doubles for the same applied voltage. This efficient push-pull operation is illustrated in Fig. 8 for a three-electrode structure on X-cut $LiNbO_3$.

As follows from the described principle of operation, the switching condition for the MZI is $\Delta\beta L = \pi$. This results in a $\sqrt{3}$ times lower switching voltage compared to that of a 2 × 2 coupler of the same interaction length L. However, there is an approximately inverse relationship between the width of the impulse responses of these switches, with the 2 × 2 coupler being the faster switch (16).

The transfer curve of an actual MZI is affected by fabrication imperfections (asymmetry of the input and output Y junctions, asymmetry of the interferometer arms, etc.) as well as waveguide loss in the structure and can be approximated by (17)

$$P_{\text{out}} = T\frac{P_{\text{in}}}{2}\left[1 + M\cos\left(\pi\frac{V}{V_\pi} + \varphi_0\right)\right] \tag{7}$$

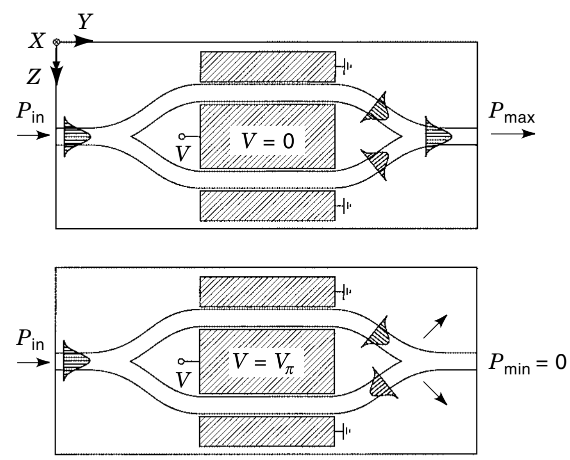

Figure 8. Principle of operation of Mach–Zehnder interferometer: maximum output produced by constructive interference (upper) and minimum transmission for out-of-phase waves in the arms (lower).

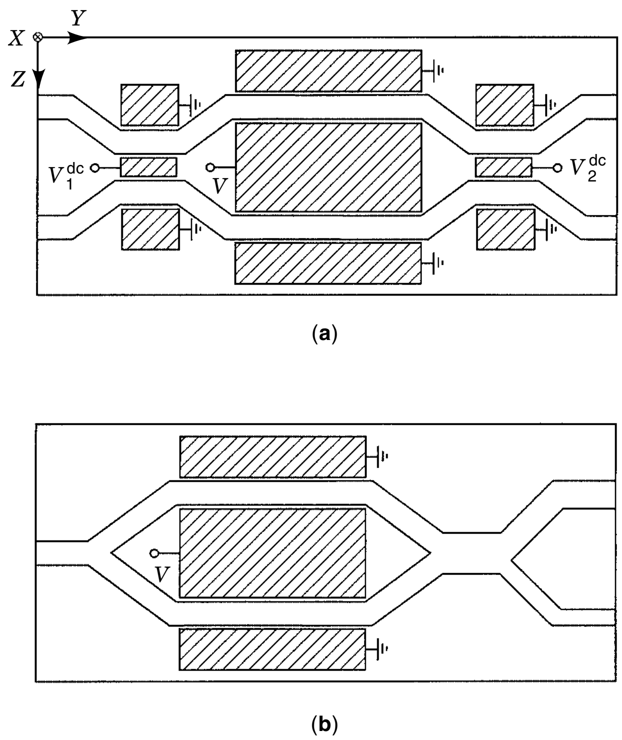

Figure 9. (a) Balanced-bridge 2 × 2 modulator (17) and (b) 1 × 2 configuration of interferometric switch (14).

where P_{in} and P_{out} are the optical power at the input and output, V_π is the half-wave voltage (i.e., the voltage required to produce a phase shift of π), φ_0 is the interferometer intrinsic phase bias, and T is a constant determined by the optical insertion loss; factor $0 \leq M \leq 1$ reflects the fact that the Y-junctions are not symmetric and the modulation depth is reduced as a result.

The performance of MZI in the conventional embodiment (Fig. 8) is known to be rather insensitive to fabrication imperfections as long as the single-mode regime of its arms is established and the output section is long enough to operate as an efficient spatial filter for the antisymmetric mode. However, the extinction ratio (i.e., the minimum-to-maximum output ratio) is rather limited as a result of fabrication imperfections, in particular, the unequal splitting of power in the Y junctions. This problem can potentially be solved by replacing one or both the Y junctions (with fixed splitting ratios) with electrically controlled DCs in the scheme of the balanced bridge modulator (17) as shown in Fig. 9(a). Advantageously, additional input/output channels also become available, enabling the device to operate as a 1 × 2 or 2 × 2 switch of discrete channels rather than an on–off, 1 × 1 switch. A dual-output MZI can also be implemented if the arms converge into a wider, two-mode section followed by an additional asymmetric Y junction [Fig. 9(b)], which operates as a mode splitter (14).

Currently, interferometric modulators are available from several vendors. Total insertion loss of a device pigtailed to single-mode fibers is as low as 3 dB. Maximum bandwidths of commercial modulators with traveling-wave electrodes (see section entitled "Optimization of High-Speed Operation") are up to 18 GHz with a typical 1.4 GHz/V ratio. Maximum power handling and extinction ratio are 200 mW and −30 dB, respectively (15).

TOTAL INTERNAL REFLECTION SWITCH

The total internal reflection (TIR) switch is composed of two pairs of input/output channels (Fig. 10) and a wide center section (18). A pair of uniform electrodes is placed in the middle of the wide section. For no applied voltage, light launched into one of the input channels emerges in the opposite, cross-state (⊗) channel. When a voltage is applied with such polarity that the local refractive index decreases in the area between the electrodes, light undergoes total internal reflection at the higher-index/lower-index interface, and the reflected light emerges in the bar-state (⊜) channel, provided that the following condition is satisfied (18):

$$\theta_i \geq \theta_c = \sin^{-1}\left\{1 - \frac{1}{2}n^2 r\Gamma\left(\frac{V}{G}\right)\right\} \tag{8}$$

where θ_i and θ_c are the angle of incidence and the critical angle, respectively (Fig. 10).

As seen from Eq. (8), the shallower the angle between the incident beam and the X axis, the lower the switching voltage. In practice, the angle θ_i is normally chosen to be close to 90°. Clearly, the switch can be made polarization-insensitive once the condition of TIR [Eq. (8)] is met for both polarizations. Devices with switching voltages from 25 V to 50 V (3.4 mm long electrodes) at the wavelength $\lambda = 0.6328$ μm were demonstrated in $LiNbO_3$ with crosstalk levels of about −15 dB

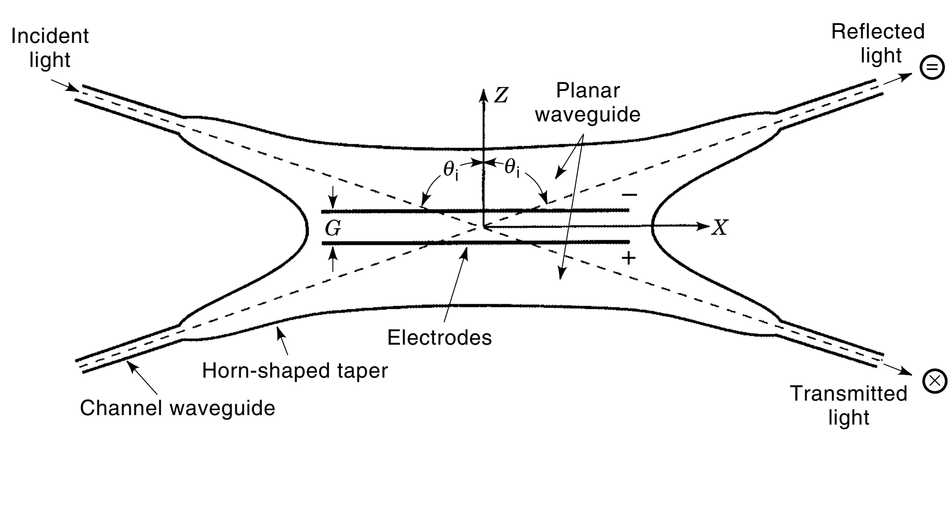

Figure 10. Schematic of TIR modulator (18). Local refractive index in the area between the electrodes can be lowered by the applied voltage V so that light undergoes total internal reflection at the higher-index/lower-index interface (top electrode) and emerges in the bar-state (⊜) channel.

(18). A TIR switch in semiconductor materials was realized in InGaAsP/InP and operated with an injection current of 20 mA (19). Since the length of the wide section and, hence, the electrodes are rather short, the device capacitance is low, and bandwidths in the gigahertz range can be achieved.

SWITCHES EMPLOYING MODE CONVERSION

This class of switches makes use of the phenomenon of mode conversion in asymmetric branches (20). An example is shown in Fig. 11 where a wide waveguide, which supports two modes, branches into two dissimilar, single-mode waveguides. The dissimilarity is normally introduced by making waveguides of unequal width. This structure is known to operate as a mode splitter provided the condition $\Delta\beta/(\gamma\theta) \gg 0.44$ is met (20), where $\Delta\beta$ is the difference between the propagation constants of the output arms considered separately, $1/\gamma$ is the average penetration depth of their modes into the area between the arms, and θ is the full branch angle. In this case, a mode of the multimode waveguide is converted into the mode of the channel with the closest propagation constant. Specifically, if the fundamental (symmetric) mode of the two-mode section is excited, it will be converted predominantly into the mode of the wider arm (arm 1 in Fig. 11). Conversely, the first-order (antisymmetric) mode of the two-moded waveguide will emerge as the mode of the narrower arm (arm 2).

Figure 12 shows a specific implementation of the described phenomenon in a digital switch that consists of two identical single-mode output waveguides and a pair of single-mode input waveguides of unequal width (21). The wider crossing area supports two modes. As always, electrodes are positioned

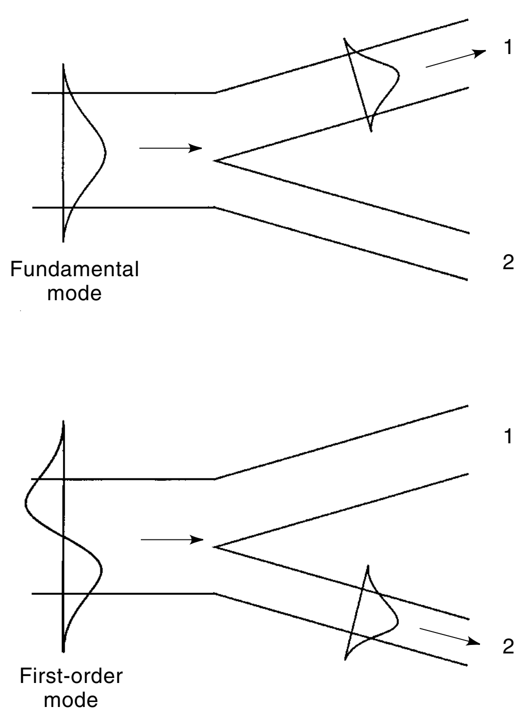

Figure 11. Asymmetric Y junction operating as a mode splitter: fundamental and first-order modes of the double-moded section are converted into the mode of the wider output channel (upper) and the narrower output channel (lower), respectively.

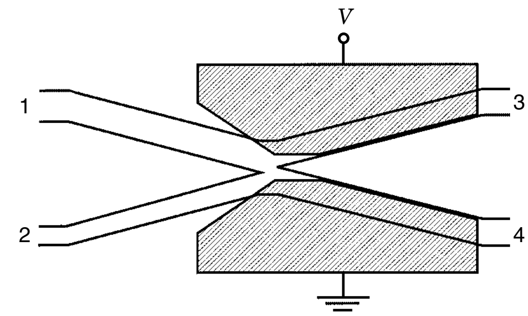

Figure 12. Asymmetric adiabatic X switch (21). For no applied voltage, light is equally split between the identical output waveguides. If a sufficiently large voltage is applied, light launched into the wider (narrower) input waveguide emerges mainly in the channel with a positive (negative) electro-optic index increment.

in order to ensure the maximum efficiency of electro-optic interaction. For example, the electrode structure in Fig. 12 corresponds to a Z-cut $LiNbO_3$ switch. The electrodes are placed over the output waveguides and extend into the wider section to provide a gradually increasing electro-optical perturbation. For no applied voltage, light is evenly split between the identical output waveguides regardless of which input waveguide is excited. Upon the application of a voltage, the symmetry of the output section is destroyed. If the voltage is large enough to satisfy the aforementioned condition for mode splitting, light launched into the wider (narrower) input waveguide will emerge in the channel with a positive (negative) electrooptical index increment. Advantageously, after the condition is met for some voltage, it will also remain satisfied upon a further increase in voltage. Hence, the transfer curve of the switch exhibits a digital-like behavior. The switching operation will be polarization-insensitive, if the switching condition is satisfied for both polarizations. Switching of TE and TM polarization with crosstalk levels better than -20 dB has been demonstrated experimentally at $\lambda = 1.52$ μm (21).

MAIN TRENDS OF DEVELOPMENT OF ELECTRO-OPTICAL MODULATORS

Currently, the primary effort is aimed at improving the linearity of the transfer curve with concomitant suppression of nonlinear distortions, at broadening the bandwidth and lowering the drive power, and at minimizing crosstalk. From a practical viewpoint, simplification of the device design and associated fabrication process is also an important consideration. Yet another trend in the development of EOMs has been generated by the desire to reduce or completely eliminate polarization dependence of device characteristics.

Linearity of Transfer Curve

The transfer curve of a conventional EO switch, including the schemes described previously, is nonlinear, typically, of a sine-like shape (Fig. 13). As a result, if a single-frequency electric signal (single tone) is applied to the electrodes, the spectrum of the modulated optical output will contain both a component at the frequency f of the modulating signal (fundamental output) and components at harmonics $2f$, $3f$, . . . (distortion) with decreasing magnitudes. In the general case of

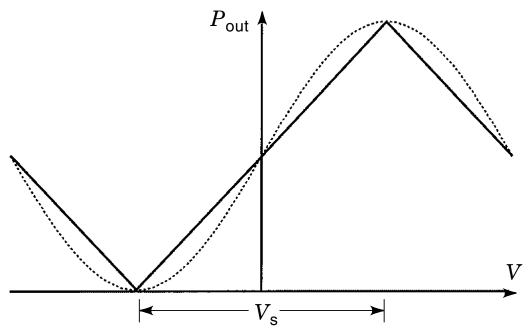

Figure 13. Triangular function representing ideal modulation characteristic and nonlinearized, sinusoidal modulation characteristic (dashed).

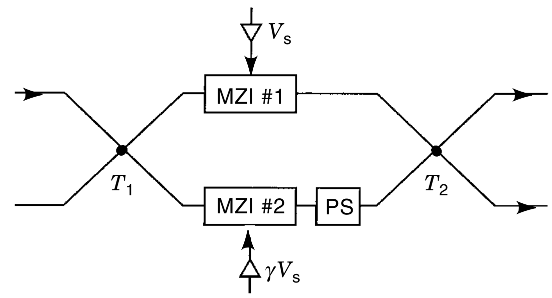

Figure 14. Dual parallel modulation technique for linearization of transfer curve. Two Mach–Zehnder modulators (MZI #1 and 2) are driven in parallel by voltages V_s and γV_s. Routing of light is accomplished by splitters/combiners T_1 and T_2. Modulated outputs are combined with a phase shift between them via a phase shifter (PS) (24).

multiple electric signals applied to the same modulator, its output will contain fundamental outputs and harmonics as well as intermodulation components at frequencies $kf_i \pm nf_j$, with f_i and f_j being the frequencies of the ith and jth tone (k and n are integers). For multioctave reception in an optical system incorporating an EOM, both the harmonic and intermodulation distortion contribute to the spurious signal and, therefore, affect the dynamic range of the system. For suboctave reception, only the intermodulation distortion should be considered, since the harmonic distortions fall outside the reception band.

Over the past decade, there has been an increasing effort aimed at developing EOMs with linearized transfer curves. A number of linearization techniques have been developed. In general, they fall into two categories, namely, electronic compensation (including predistortion compensation and feedforward compensation) and the optical methods of linearization. The latter are capable of going to higher frequencies because no electronics are used for linearization. In general, a tradeoff between the linearity of the transfer curve and the device complexity can be observed as demonstrated by the examples described later.

Linearization of the Mach–Zehnder interferometer has been achieved by the dual-polarization technique (22,23) and parallel-modulation scheme (24). In both approaches, improvement in linearity is accomplished by the summation of two modulation characteristics. The underlying idea, originally implemented in a two-section Bragg switch (25), makes use of the Fourier series of an ideal, triangular transfer function (Fig. 13) of the form

$$P_{\mathrm{tr}}(V/V_s) = \frac{4}{\pi^2} T P_{\mathrm{in}} \sum_{m=0}^{\infty} \frac{1 + (-1)^m \sin[(2m+1)\pi V/V_s]}{(2m+1)^2} \quad (9)$$

where V_s is the switching voltage (Fig. 13).

As seen from the series in Eq. (9), a triangular response can be synthesized, if one sums up sinusoidal transfer curves with appropriate amplitudes, phase biases, and periods (i.e., switching voltages). In fact, dependence Eq. (9) can be well approximated by only the first two harmonic terms. This circumstance significantly simplifies designing a linearized modulator. In the dual parallel modulation scheme, two separate modulators with half-wave voltages relating as 1 : 3 are combined (Fig. 14). The power splitting between the modulators (controlled by directional coupler T_1) is set to about 1 : 27, slightly different from 1 : 9 in Eq. (9), to ensure the highest suppression of the third-order intermodulation distortion (22,24).

The dual-polarization technique invokes a folded design in $LiNbO_3$ whereby the necessary two modulation characteristics are produced by just one MZI in which the waveguide modes of both TM and TE polarization are excited (Fig. 15). The half-wave voltage for the extraordinary (TE in Fig. 15) polarization is about three times lower than that for the ordinary (TM) polarization because of the difference $r_{33}/r_{13} \approx 3$ in the electrooptic coefficients r_{33} and r_{13}, which are responsible for the modulation of the TE and TM polarizations, respectively, by the horizontal component of the electric field. The two polarizations can be excited at the modulator input by a beam linearly polarized at an angle with the optical axis (Fig. 15). By adjusting the angle, the necessary ratio of the power in the TE-wave to that in the TM-wave can be set.

Another approach to linearization embarks on the concatenation of several modulators, MZIs, or DCs. Several schemes have been reported (26,27). By setting proper splitting ratios and interaction lengths of the incorporated elements, the third-order or even the fifth-order nonlinearity can be eliminated with the next odd-order terms limiting the dynamic range.

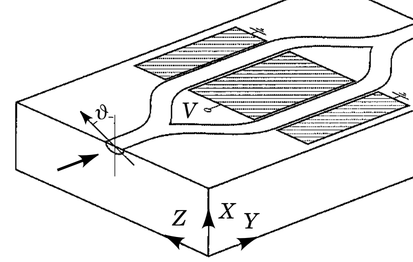

Figure 15. Linearization of the transfer curve of Mach–Zehnder interferometer by dual-polarization technique (22,23). Waveguide modes of TM and TE polarization are excited in the same waveguide. The transfer curve can be linearized by properly adjusting the amplitudes and phase biases of the TE and TM waves. The relative amplitudes are varied by adjusting the angle τ of the polarization plane of the incident linearly polarized beam.

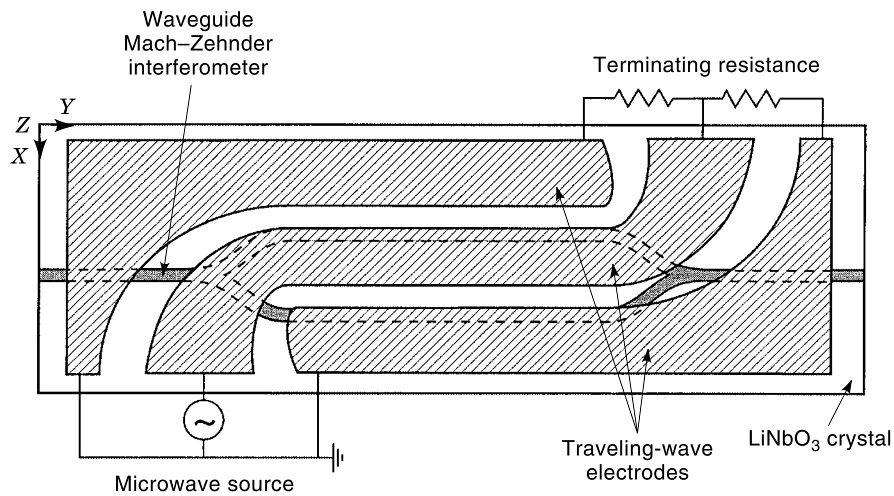

Figure 16. Traveling-wave Mach–Zehnder modulator. The electrode structure is used as an extension of the driving transmission line from the microwave source and is terminated by a matching resistance. The microwave travels along the electrode structure and modulates the guided wave propagating through the waveguide.

Optimization of High-Speed Operation

High-speed operation of an EOM is characterized by its optical frequency response, viz., the magnitude of the modulated component in the optical output versus the frequency of the modulating electric signal. The phase response (i.e., the dependence of the phase of the optical output on frequency) is also an important characteristic that determines the chirp of the device. For a baseband modulator, the bandwidth is normally defined as the frequency at which the optical response rolls off by 3 dB from its dc value. The bandwidth of a bandpass modulator is defined by the two frequencies at which the optical response rolls off by 3 dB from its value at the center frequency.

A trade-off is known to exist between the bandwidth and length of an EOM. As a consequence, higher modulation speeds can be achieved with a shorter interaction length, however, at the expense of a higher modulating power required to maintain the same modulation depth. The maximum bandwidth × length product is determined by the specific type, lumped or traveling wave, of the electrode structure. The electrode length of the lumped-type modulator is small compared to the wavelength of the modulating electric signal. The electrode structure appears as a lumped-element capacitor with the bandwidth Δf limited primarily by the electrode capacitance C in accordance with $\Delta f = 1/(2\pi RC)$, where R is the load resistance. The capacitance is proportional to the electrode length leading to a bandwidth × length product of approximately 2.2 GHz · cm in $LiNbO_3$.

More efficient high-speed modulation can be attained by using traveling-wave EOMs. In this case, the electrode structure is used as an extension of the driving transmission line from a microwave source. The electrode structure of a typical traveling-wave EOM is a microstrip line formed by two (asymmetric line) or three (symmetric line) electrodes. The former is called the coplanar strip (CPS) electrode while the latter is the coplanar waveguide (CPW) structure. Figure 16 illustrates a traveling-wave Mach–Zehnder interferometer with a CPW electrode. The microwave and the optical mode propagate codirectionally and, in general, with different velocities. The velocity mismatch and radiofrequency (RF) loss are the major factors limiting the bandwidth of a traveling-wave EOM. The velocity mismatch is determined by the properties of the substrate material, namely, its dielectric constant at the microwave and optical frequencies. In lithium niobate, for example, the microwave travels along a thin electrode line about two times slower than the optical mode propagates through the waveguide. The situation is opposite in semiconductor modulators (GaAs/AlGaAs, etc.) where the microwave is about 30% faster than the optical wave.

As a result of velocity mismatch, the local electrooptical phase shift $\Delta\varphi$ accumulated over a short distance Δz is a periodic function (Fig. 17) of position z along the propagation direction (28):

$$\Delta\varphi = \Delta\beta_0 \cos\left[2\pi f\left(\frac{zN_m\gamma}{c} - t\right)\right]\Delta z \qquad (10)$$

with $\gamma = 1 - N_o/N_m$ and $\Delta\beta_0 = -(\pi N_o^3 r \Gamma V_0)/\lambda G$, where N_o and N_m are the indices of the optical mode and the microwave, respectively; f is the microwave frequency; c is the speed of light in a vacuum; r denotes the effective electrooptic coefficient; Γ is the electrooptical overlap integral; V_0 is the magnitude of the microwave; λ is the free-space optical wavelength; and G is the inter-electrode gap.

Under a small-signal approximation, the frequency response is proportional to the frequency dependence of the total phase $\Delta\Psi$ accumulated over the entire interaction length

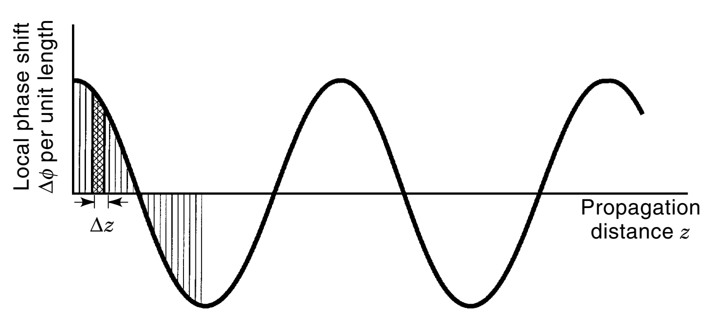

Figure 17. Oscillating local phase shift vs. propagation distance results from the velocity mismatch between the microwave and optical mode.

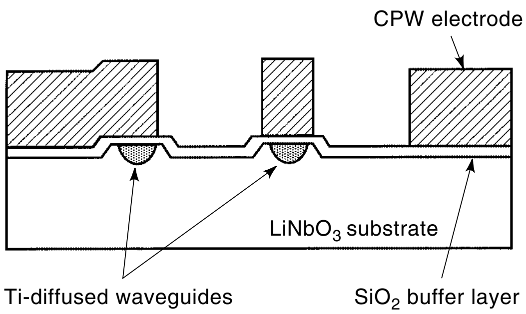

Figure 18. Velocity-matched Mach–Zehnder modulator with ridge waveguides, ultrathick traveling-wave electrodes, and thick buffer layer (33). The ultra-thick electrodes pull the microwave field out of the $LiNbO_3$ substrate with high dielectric constants to lower the average microwave index and bring it close to that of the optical mode. A thick buffer layer should be used to keep the impedance around 50 Ω.

L (28):

$$\Delta\Psi(f) = \int_0^L \frac{\Delta\varphi(t, z)}{\Delta z}\, dz = \Delta\beta_0 L \frac{\sin(\theta/2)}{(\theta/2)} \cos[\theta/2 - 2\pi f t] \tag{11}$$

where

$$\theta(f) = \frac{\pi f}{f_c} \quad \text{and} \quad f_c = \frac{c}{2N_m L\gamma}$$

As seen from Eq. (11), the frequency response is of the form $(\sin x)/x$ with a bandwidth of $\sim f_c$. For example, $\gamma \sim 0.5$ in lithium niobate results in a bandwidth × length product of about 9.6 GHz · cm. In Eqs. (10) and (11), the RF loss caused by the finite conductivity of the metal electrode is not accounted for. For a given electrode geometry, the attenuation coefficient of the microwave increases with frequency as $\sim\sqrt{f}$ because of the decreasing skin depth and may become a factor significantly affecting the frequency response, especially at high frequencies. Experimental values of RF attenuation coefficients for Au/Cr electrodes are typically in the range from 0.3 $dB \cdot cm^{-1} \cdot GHz^{-1/2}$ to 0.7 $dB \cdot cm^{-1} \cdot GHz^{-1/2}$.

There are a number of techniques to further improve the high-speed operation of traveling-wave EOMs. These techniques fall into two categories, namely, true velocity matching and quasi-phase matching (QPM). True velocity matching can be achieved in a straightforward manner in materials with close N_o and N_m such as, for example, polymers (29). MZIs in poled polymers have demonstrated bandwidths up to 94 GHz with further improvements expected. In ferroelectrics, ultra-thick electrodes (30,31) have been employed, in combination with a shielding plane (32) or ridge waveguides (33), to pull the microwave field out of the substrate with high dielectric constants. If more of the microwave field propagates in air, the average microwave index decreases and can be tuned to that of the optical mode by properly adjusting the electrode thickness. Since the electrode impedance also decreases upon increasing the electrode thickness, a thick buffer layer should be used to bring the impedance back to ~50 Ω. For perfect velocity matching, the electrode RF loss is the dominant factor limiting the device bandwidth. Figure 18 shows the cross-section of a velocity-matched MZI with ultra-thick electrodes and ridge waveguides etched in $LiNbO_3$. A 3 dB (optical) bandwidth of ~100 GHz was reported with a dc half-wave voltage of 5.1 V at $\lambda = 1.55\ \mu m$ (33). In semiconductors, slow-wave electrode structures achieved true velocity matching by slowing down the microwave through capacitance loading of the microwave line. A GaAs/AlGaAs modulator with a bandwidth in excess of 40 GHz and a 16.8 V drive voltage at $\lambda = 1.55\ \mu m$ was reported (34).

The principle of the second approach, namely QPM, is to invert, by some means, the negative "half-periods" of the oscillating dependence of the local phase shift (Fig. 19), which reduce the modulation efficiency (28). The conventional implementation is electrode phase reversals (28) positioned at points where the microwave and the optical mode become 180° out of phase because of the walk-off [Fig. 20(a)]. Alternately, the position of the waveguide can be periodically switched with respect to the interelectrode gap to produce the phase reversals necessary for QPM. At the reversal, the direction of the electric field within the wave-guiding area is reversed, adding a phase shift of π to the same shift accumulated, because of the velocity mismatch, over the distance between consecutive reversals. The microwave and optical mode are, therefore, brought in phase.

By employing QPM, the frequency response can be tailored to be baseband or bandpass. With periodic (equidistant) reversals, a bandpass response can be achieved (28). The center frequency is uniquely determined by the period of reversals and can be designed to be arbitrarily high. Because all the segments operate synchronously at the center frequency, efficiency can be increased by adding more electrode segments. In practice, both the maximum center frequency and modulation efficiency are limited by the RF loss because of the finite conductivity of the metal electrode. A bandpass modulator on Z-cut $LiNbO_3$ with periodic electrode phase reversals demonstrated a 20 GHz response centered at 40 GHz (35). A periodic reversal patterns have also been realized in experimental devices that demonstrated spread frequency spectra with increased bandwidth × length products (36). A flat response, either baseband or bandpass, can be synthesized with alternating electrooptical interaction profiles (37). Deteriorated performance in the time domain caused by the nonlinear phase response, inherent to aperiodic sequences, may be remedied by cascaded schemes incorporating several modulators.

Another embodiment of QPM is EOMs in ferroelectrics with domain reversals [Fig. 20(b)]. Instead of reversing the direction of the electric field with respect to the optical axis,

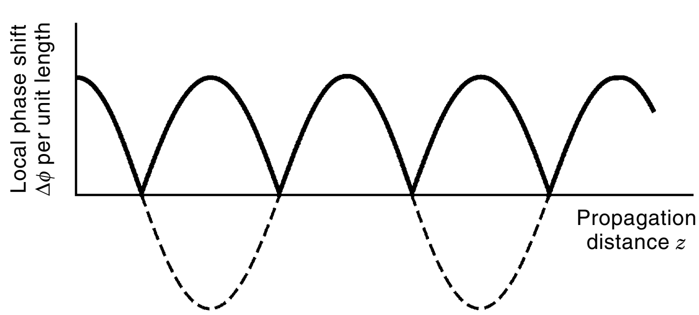

Figure 19. Principle of quasi-phase matching: negative half-periods (dashed) are somehow inverted. Total accumulated phase shift (total area under the solid curve) increases as a result of the inversion.

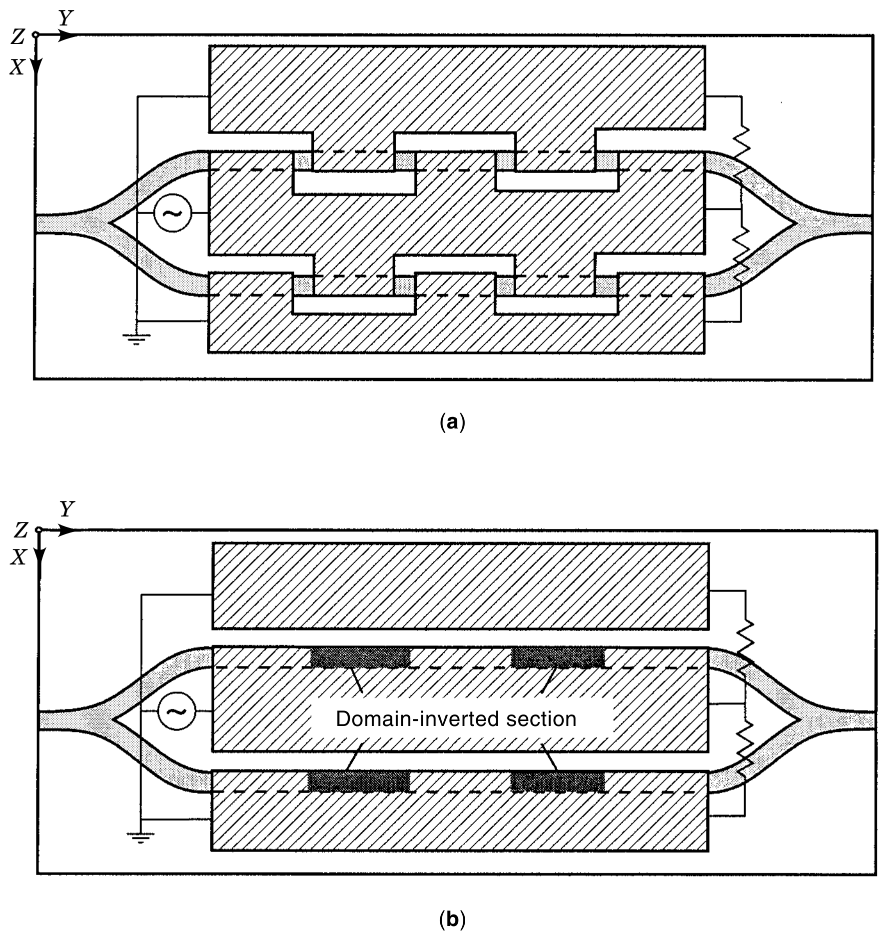

Figure 20. Quasi-phase-matched Mach–Zehnder modulator with electrode reversals (a) (28) and domain reversals (b) (38). The latter uses a uniform electrode structure to achieve QPM and can be implemented in both Z-cut $LiNbO_3$ (b) and X-cut $LiNbO_3$ (not shown).

the latter is reversed to produce the necessary phase reversal (38). Advantageously, this scheme can be implemented with a three-electrode, push–pull electrode structure in both Z- and X-cut crystals. Devices in X-cut are known to benefit from the temporal and thermal stability inherent to this crystal orientation. On the other hand, electrode phase reversals in X cut would require more than three electrodes for push–pull operation, which would complicate the matching of the electrode structure to a single microwave source significantly.

Polarization-Independent Operation

The performance of a typical EOM is dependent on the state of polarization of incoming light as a result of two main factors. First, the orthogonal polarizations (TE and TM) see unequal electrooptical coefficients. For instance, in a modulator in Z-cut $LiNbO_3$, TM and TE polarization will be controlled by r_{33} and r_{13} coefficients, respectively, with the ratio r_{33}/r_{13} being about 3. The same applied voltage will produce an approximately three times larger electrooptical index change for TM polarization than for TE polarization. Second, waveguide index profiles are typically anisotropic as a result of the material and waveguide birefringence as well as the possible difference in the waveguide index increments for the two polarizations. Consequently, the fields and the propagation constants of the optical modes depend on the state of polarization. Thus, the transfer curve of the switch is polarization-dependent. On the other hand, polarization-independent operation of the switch is strongly preferred because the standard, circular fiber that does not preserve polarization is the least expensive option for long-haul communication links. Advantageously, the impact of the polarization hole burning (anisotropic gain saturation) in erbium-doped fiber amplifiers can be minimized by using polarization scramblers in such polarization-independent optical links. Therefore, polarization-insensitive modulators are often the preferred choice, even though there is normally a voltage penalty compared to the conventional (single polarization) modulators.

There are two possible approaches to the problem of polarization dependence. First, materials with reduced birefringence can be used. For example, polymers are known to exhibit reduced birefringence. In semiconductors, polarization-independent devices have been demonstrated where the material and waveguide birefringence had been compensated for by employing multiple-quantum-well structures. The remaining source of the polarization dependence of switching characteristics comes from the anisotropy in the electro-optical properties. Second, structural modifications have been proposed to realize polarization independence. These include structures with weighted coupling (39), switches with $\Delta\beta$ and $\Delta\kappa$ modulation (40), multiple electrodes (41), special crystal orientation (42), and structures with tensile strain (43).

In directional couplers with weighted coupling (Fig. 21), the interaction strength profile (coupling coefficient) is apodized by varying the interwaveguide gap along the propagation

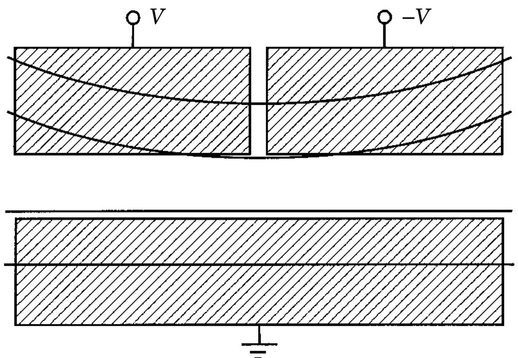

Figure 21. Polarization-independent directional coupler with weighted coupling (39). Proper apodization (weighting function) can produce complete switching for both TE and TM polarization at the same applied voltage.

direction so as to achieve the same coupling coefficient for both polarizations. In this case, the cross state for the TE- and TM-modes can be achieved simultaneously. The bar state is tuned electro-optically. Despite the anisotropy in the electro-optical coefficients, crosstalk below −23 dB has been achieved for the two polarizations in a Z-cut $LiNbO_3$ device with reversed $\Delta\beta$ electrodes and a Hamming function for the coupling coefficient (39).

In Mach–Zehnder interferometers, polarization independence can be achieved with a structure incorporating a dual set of electrodes (44). A symmetric waveguide interferometer is formed in a Z-cut X-propagating $LiNbO_3$ substrate (Fig. 22). For no applied voltage, the switch is on for both polarizations as a result of the symmetry of the structure. TE polarization is modulated by both the electrode sets via the r_{22} and r_{13} coefficients. On the other hand, TM polarization is controlled via the electro-optical coefficient r_{33} by only one electrode set, with the electrodes on top of the interferometer arms. The lengths of the sections can be chosen so as to compensate for the difference in the electro-optical coefficients and achieve a phase shift of π for both polarizations at the same applied voltage.

Polarization-insensitve operation can also be achieved by using the principle of polarization diversity which invokes parallel processing (modulation) of each polarization independently (45). Normally, two polarization splitters are required to first separate and then recombine the polarizations. The TM and TE components of light at the input are routed to different channels and independently modulated by two modulators, each of which is optimized for one polarization. If the modulated TM and TE components are subsequently recombined in the other polarization splitter/combiner at the output, a state of polarization identical to that at the input is produced.

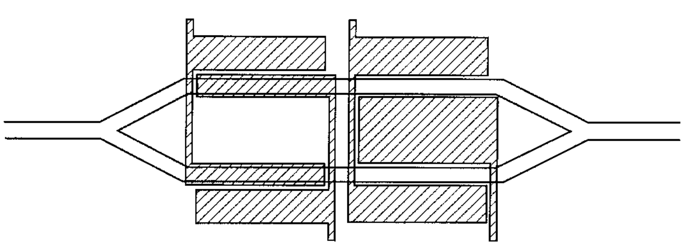

Figure 22. Polarization-independent Mach–Zehnder interferometer in Z-cut $LiNbO_3$ (44). The left section modulates guided modes of both TM and TE polarization while the right section modulates only the TE-polarized mode. For no voltage, the switch is on (maximum transmission) for both polarizations. Voltage can be selected to turn the switch off (minimum transmission) simultaneously for both TM and TE polarization.

Minimization of Insertion Loss

From a practical standpoint, it is most imperative to minimize the insertion loss of an EOM to be deployed in a system because reduced loss directly translates into increased spans of amplifier-free transmission. There are three main factors contributing to the insertion loss, namely, propagation loss, loss at bends and tapers, and coupling loss. Propagation loss along the waveguide structure is caused by the bulk absorption in the material and scattering at interfaces. By controlling impurities and by refining the growth technology, bulk absorption can be brought down to a negligibly low level. As a result, the propagation loss in both dielectric and semiconductor materials is largely determined by the scattering at the substrate/air interface. By refining the technology of waveguide fabrication, propagation loss as low as 0.05 dB/cm in ferroelectrics (46), 0.004 dB/cm in polymers (2), and 0.2 dB/cm in semiconductors (47), all at $\lambda = 1.5$ μm, have been achieved.

Loss at waveguide bends, junctions and tapers can be minimized by improving mode confinement and optimizing waveguide topology. Typical losses are of the order of a fraction of a decibel. Special techniques have yielded low losses even in structures with abrupt corners or small-radius bends.

Reliable coupling of integrated-optic devices with optical fibers has long been the major hindrance in wide-scale deployment of EOMs. In the case of single-mode fibers, the demands on the coupling/connectorization technology are most stringent because of the small transversal dimensions of the fiber and waveguide modes. Eventually, a number of techniques have been developed and refined to produce high yield based on a manual or semiautomatic process. Currently, EOMs pigtailed to multimode or single-mode fiber are commercially available from several vendors (15). Pigtailed devices have a total insertion loss of several decibels with a coupling loss of typically less than 1 dB; they meet stringent requirements on the usable temperature range, maximum acceleration, etc.

CONCLUSION

Electro-optical modulators/switches represent a formidable area of integrated optics where a multitude of schemes have been proposed, developed, and tested. A number of EOMs are already available commercially. Advanced devices are being developed and optimized. Bandwidths up to 100 GHz with TTL-compatible voltages have been demonstrated. Techniques for coupling EOMs to optical fibers, including single-mode fibers, have been established paving the way to a vast variety of practical applications. Current effort is aimed at improving the linearity of the transfer curve with concomitant reduction in nonlinear distortions, at broadening the bandwidth, and at minimizing polarization dependence. From a practical viewpoint, simplification of the device design and the associated fabrication process is of paramount importance. Future optical systems of signal transmission and processing, including CATV and radar antenna remoting, will continue to enjoy the benefits that advanced EOMs are able to offer.

BIBLIOGRAPHY

1. G. E. Bodeep and T. E. Darcie, Semiconductor lasers versus external modulators: A comparison of nonlinear distortion for lightwave subcarrier CATV applications, *IEEE Photon. Technol. Lett.,* **1** (11): 401–403, 1989.
2. R. G. Hunsperger, *Integrated Optics: Theory and Technology,* Berlin: Springer-Verlag, 1995, 4th ed.
3. C. H. Bulmer, Sensitive, highly linear lithium niobate interferometers for electromagnetic field sensing, *Appl. Phys. Lett.,* **53**: 2368–2370, 1988; D. H. Naghski et al., An integrated photonic Mach-Zehnder interferometer with no electrodes for sensing electric fields, *J. Lightw. Technol.,* **12** (6): 1092–1098, 1994.
4. M. Nazarathy et al., Progress in externally modulated AM CATV transmission systems, *J. Lightw. Technol.,* **LT-11** (1): 82–105, 1993.
5. H. Zmuda and E. N. Toughlian, *Photonic Aspects of Modern Radar,* Boston: Artech House, 1994.
6. P. J. Duthie and M. J. Wale, 16 × 16 single chip optical switch array in lithium niobate, *Electron. Lett.,* **27**: 1265–1266, 1991.
7. S. E. Miller, Coupled-wave theory and waveguide applications, *Bell Syst. Tech. J.,* **33**: 661–719, 1954; see also E. A. J. Marcatili, Dielectric rectangular waveguide and directional coupler for integrated optics, *ibid.,* **48**: 2071–2102, 1969.
8. H. Kogelnik and R. V. Schmidt, Switched directional couplers with alternating $\Delta\beta$, *IEEE J. Quantum Electron.,* **QE-12** (7): 396–401, 1976.
9. S. A. Samson, R. F. Tavlykaev, and R. V. Ramaswamy, Two-section reversed $\Delta\beta$ switch with uniform electrodes and domain reversal, *IEEE Photon. Technol. Lett.,* **9** (2): 197–199, 1997.
10. S. Thaniyavarn, Modified 1 × 2 directional coupler waveguide modulator, *Electron. Lett.,* **22** (18): 941–942, 1986.
11. S. Thaniyavarn, *A synthesized digital switch using a 1 × 2 directional coupler with asymmetric $\Delta\beta$ phase reversal electrode, Integrated and Guided-Wave Optics'88,* Santa Fe, NM, Tech. Dig. Ser., 1988, Vol. 5, Paper TuC6.
12. M. Papuchon, A. Roy, and D. B. Ostrowsky, Electrooptically active optical bifurcation: BOA, *Appl. Phys. Lett.,* **31** (4): 266–267, 1977.
13. R. A. Forber and E. Marom, Symmetric directional coupler switches, *IEEE J. Quantum Electron.,* **QE-22** (6): 911–919, 1986.
14. W. E. Martin, A new waveguide switch/modulator for integrated optics, *Appl. Phys. Lett.,* **26** (10): 562–564, 1975.
15. United Telecommunications Products, *Catalog of Integrated Optical Circuits,* 1997 Bloomfield, CT 06002; see also AT&T Microelectronics, *Lithium Niobate SLIM-PAC Electro-optic Modulator,* Advanced data sheet, 1996, Allentown, PA 18103.
16. S. K. Korotky and R. C. Alferness, Time- and frequency-domain response of directional-coupler traveling-wave optical modulators, *J. Lightw. Technol.,* **LT-1** (1): 244–251, 1983.
17. V. Ramaswamy, M. D. Divino, and R. D. Standley, Balanced bridge modulator switch using Ti-diffused $LiNbO_3$ strip waveguides, *Appl. Phys. Lett.,* **32**: 644–646, 1978.
18. C. S. Tsai, B. Kim, and F. R. El-Akkari, Optical channel waveguide switch and coupler using total internal reflection, *IEEE J. Quantum Electron.,* **QE-14** (7): 513–517, 1978.
19. K.-R. Oh et al., A very low operation current InGaAsP/InP total internal reflection optical switch using p/n/p/n current blocking layers, *IEEE Photon. Technol. Lett.,* **6** (1): 65–67, 1994.
20. W. K. Burns and A. F. Milton, Waveguide transitions and junctions, in T. Tamir (ed.), *Integrated Optics,* Berlin: Springer-Verlag, 89–144, 1988.
21. Y. Silberberg, P. Perlmutter, and J. E. Baran, Digital optical switch, *Appl. Phys. Lett.,* **51** (16): 1230–1232, 1987.
22. L. M. Johnson and H. V. Rousell, Reduction of intermodulation distortion in interferometric optical modulators, *Opt. Lett.,* **13** (10): 928–930, 1988.
23. E. M. Zolotov and R. F. Tavlykaev, Integrated optical Mach-Zehnder modulator with a linearized modulation characteristic, *Sov. J. Quantum Electron.,* **18** (3): 401–403, 1988.
24. S. K. Korotky and R. M. Ridder, Dual parallel modulation scheme for low-distortion analog optical transmission, *IEEE J. Sel. Areas Commun.,* **8** (7): 1377–1381, 1990.
25. P. R. Ashley and W. S. C. Chang, Linearization technique for a guided-wave electro-optic Bragg modulator, in *Digest of Topical Meeting on Integrated and Guided-Wave Optics* Atlanta, GA: Optical Society of America, 1986, pp. 36–38.
26. H. Skeie and R. V. Johnson, Linearization of electro-optic modulators by a cascade coupling of phase modulating electrodes, *Proc. SPIE,* **1583**: 153–164, 1991.
27. D. Raskin, K. Chiang, and J. B. Stamatoff, *Cable system incorporating highly linear optical modulator,* U.S. Parent No. 5,031,235, 1991.
28. R. C. Alferness, S. K. Korotky, and E. A. J. Marcatili, Velocity-matching techniques for integrated-optic traveling-wave switch modulators, *IEEE J. Quantum Electron.,* **QE-20** (3): 301–309, 1984.
29. S. Kalluri et al., Monolithic integration of waveguide polymer electrooptic modulators on VLSI circuitry, *IEEE Photon. Technol. Lett.,* **8** (5): 644–646, 1996.
30. M. Seino et al., *33-GHz-cm broadband Ti:$LiNbO_3$ Mach-Zehnder modulator, ECOC Tech. Dig.,* 1989, Paper ThB22-5.
31. G. K. Gopalakrishnan et al., Performance and modeling of broadband $LiNbO_3$ traveling wave optical intensity modulators, *J. Lightw. Technol.,* **12** (10): 1807–1819, 1994.
32. K. Kawano, High-speed shielded velocity-matched Ti:$LiNbO_3$ optical modulator, *IEEE J. Quantum Electron.,* **QE-29** (9): 2466–2475, 1993.
33. K. Noguchi, O. Mitomi, and H. Miyazawa, Low-voltage and broadband Ti:$LiNbO_3$ modulators operating in the millimeter wavelength region, *Proc. Opt. Fiber Commun. Conf.,* 1996, Paper ThB2, pp. 205–206.
34. R. Spickermann et al., GaAs/AlGaAs traveling wave electro-optic modulator with an electrical bandwidth $>$ 40 GHz, *Electron. Lett.,* **32** (12): 1095–1096, 1996.
35. S. K. Korotky and J. J. Veselka, Efficient switching in a 72-Gbit/s Ti:$LiNbO_3$ binary multiplexer/demultiplexer, *Tech. Dig. Conf. Opt. Fiber Commun.,* San Francisco, 1990, Paper TuH2, p. 32.
36. M. Nazarathy, D. W. Dolfi, and R. L. Jungerman, Spread spectrum frequency response of coded phase reversal traveling-wave modulators, *J. Lightw. Technol.,* **LT-5**: 1433–1443,1987.
37. E. M. Zolotov, V. M. Pelekhatyi, and R. F. Tavlykaev, Broadening the bandwidth and increasing the efficiency of traveling-wave integrated-optic modulators, *Int. J. Optoelectron.,* **5**: 503–512, 1990.
38. W. Wang, R. Tavlykaev, and R. V. Ramaswamy, Bandpass traveling-wave Mach-Zehnder modulator in $LiNbO_3$ with domain reversal, *IEEE Photon. Technol. Lett.,* **9** (5): 610–612, 1997.
39. R. C. Alferness, Polarization-independent optical directional coupler switch using weighted coupling, *Appl. Phys. Lett.,* **35**: 748–750, 1979.

40. P. Granestrand and L. Thylen, Polarization independent switch and polarization splitter employing $\Delta\beta$ and $\Delta\kappa$ modulation, *Electron. Lett.,* **24**: 1142–1143, 1988.
41. P. Granestrand, Four-sectioned polarization-independent directional coupler with extremely relaxed fabrication tolerances, *IEEE Photon. Technol. Lett.,* **4** (6): 594–596, 1992.
42. K. Komatsu et al., Polarization-independent GaAs/AlgaAs electro-optic guided-wave directional coupler switch using (111)-oriented GaAs substrate, *OSA Proc. Photon. Switch.,* **8**: 24–27, 1991.
43. T. Aizawa et al., Polarization-independent switching operation in directional coupler using tensile-strained multi-quantum well, *IEEE Photon. Technol. Lett.,* **7** (1): 47–49, 1995.
44. W. K. Burns et al., Interferometric waveguide modulator with polarization-independent operation, *Appl. Phys. Lett.,* **33**: 944–947, 1978.
45. B. Glance, Polarization independent coherent optical receiver, *J. Lightw. Technol.,* **LT-5** (2): 274–276, 1987.
46. F. Tian et al., Polarization-independent integrated optical, acoustically tunable double-stage wavelength filter in $LiNbO_3$, *J. Lightw. Technol.,* **LT-12** (7): 1192–1197, 1994.
47. J. H. Angenent et al., Extremely low loss InP/GaInAsP rib waveguides, *Electron. Lett.,* **25** (10): 628–629, 1989.

R. F. TAVLYKAEV
R. V. RAMASWAMY
University of Florida

ELECTRO-OPTIC CRYSTALS. See PHOTOREFRACTIVE EFFECT.

ELECTRO-OPTICS, INTEGRATED. See INTEGRATED OPTOELECTRONICS.